Nonadiabatic coupling of the dynamical structure to the superconductivity in $YSr_2Cu_{2.75}Mo_{0.25}O_{7.54}$ and $Sr_2CuO_{3.3}$

Steven D. Conradson[a,b,1], Theodore H. Geballe[c,1], Chang-Qing Jin[d,e,1], Li-Peng Cao[d,e], Andrea Gauzzi[f,1], Maarit Karppinen[g,1], Gianguido Baldinozzi[h], Wen-Min Li[d,e], Edmondo Gilioli[i], Jack M. Jiang[c,j], Matthew Latimer[k], Oliver Mueller[k], and Venera Nasretdinova[a,l]

[a]Department of Complex Matter, Jozef Stefan Institute, 1000 Ljubljana, Slovenia; [b]Department of Chemistry, Washington State University, Pullman, WA 99164; [c]Department of Applied Physics, Stanford University, Stanford, CA 94305; [d]Institute of Physics, Chinese Academy of Sciences, 100864 Beijing, China; [e]School of Physics, University of Chinese Academy of Sciences, Chinese Academy of Sciences, Beijing 100190, China; [f]IMPMC, Sorbonne Université and CNRS, 75005 Paris, France; [g]Department of Chemistry and Materials Science, Aalto University, FI-00076 Aalto, Finland; [h]Structures, Properties and Modeling of Solids Laboratory, CNRS CentraleSupélec, Université Paris-Saclay, F-91192 Gif-sur-Yvette, France; [i]Institute of Materials for Electronics and Magnetism, Consiglio Nazionale delle Ricerche, A-43124 Parma, Italy; [j]Stanford Institute for Materials and Energy Sciences, SLAC National Accelerator Laboratory, Menlo Park, CA 94025; [k]Stanford Synchrotron Radiation Lightsource, SLAC National Accelerator Laboratory, Menlo Park, CA 94025; and [l]Center of Excellence in Nanoscience and Nanotechnology, Jozef Stefan Institute, 1000 Ljubljana, Slovenia

Contributed by Theodore H. Geballe, November 8, 2020 (sent for review August 31, 2020; reviewed by Antonio Bianconi, Jochen Mannhart, and Naurang Saini)

A crucial issue in cuprates is the extent and mechanism of the coupling of the lattice to the electrons and the superconductivity. Here we report Cu K edge extended X-ray absorption fine structure measurements elucidating the internal quantum tunneling polaron (iqtp) component of the dynamical structure in two heavily overdoped superconducting cuprate compounds, tetragonal $YSr_2Cu_{2.75}Mo_{0.25}O_{7.54}$ with superconducting critical temperature, T_c = 84 K and hole density p = 0.3 to 0.5 per planar Cu, and the tetragonal phase of $Sr_2CuO_{3.3}$ with T_c = 95 K and p = 0.6. In $YSr_2Cu_{2.75}Mo_{0.25}O_{7.54}$ changes in the Cu-apical O two-site distribution reflect a sequential renormalization of the double-well potential of this site beginning at T_c, with the energy difference between the two minima increasing by ∼6 meV between T_c and 52 K. $Sr_2CuO_{3.3}$ undergoes a radically larger transformation at T_c, >1-Å displacements of the apical O atoms. The principal feature of the dynamical structure underlying these transformations is the strongly anharmonic oscillation of the apical O atoms in a double-well potential that results in the observation of two distinct O sites whose Cu–O distances indicate different bonding modes and valence-charge distributions. The coupling of the superconductivity to the iqtp that originates in this nonadiabatic coupling between the electrons and lattice demonstrates an important role for the dynamical structure whereby pairing occurs even in a system where displacements of the atoms that are part of the transition are sufficiently large to alter the Fermi surface. The synchronization and dynamic coherence of the iqtps resulting from the strong interactions within a crystal would be expected to influence this process.

X-ray absorption fine structure | cuprates | superconductivity | dynamical structure | tunneling polarons

More than 30 y after the discovery of unconventional superconductivity in cuprates (1) and subsequently in analogous materials its underlying mechanism and in particular the role of the lattice are still under debate. Proposed microscopic theories range from purely electronic Mott–Hubbard and t-J approaches at one extreme to Bose–Einstein condensates of bipolarons at the other (2–4). Experimentally, however, anomalous isotope effects (5), resonant ultrasound (6), angle-resolved photoemission spectroscopy (7–9), femtosecond optical pump terahertz (10)/megaelectron-volt transmission electron microscopy probe (11), infrared pump (12), and so on have demonstrated that specific phonons not only couple to the superconductivity but correlate directly with the gap energy and may even transiently induce it well above the superconducting critical temperature, T_c. Cuprates also exhibit a plethora of superstructures indicative of strong electron–lattice coupling, stripes that have been proposed to stabilize the superconductivity (13), and charge-density waves (14, 15) and the pseudogap (PG) (16) that compete with it. Another possibility is mechanisms that boost T_c from a low value expected within a conventional Bardeen-Cooper-Schrieffer (BCS) scheme. That this question remains unanswered suggests considering more unconventional approaches (4). One candidate is the dynamical structures of cuprates, $S(Q, E)$ or experimentally $S(Q, t = 0)$, specifically their internal quantum tunneling polarons (iqtp). An iqtp is a set of atoms oscillating between two structures that possess different geometries, energy levels, and charge distributions (17–19). A chemist would describe these endpoints as separate species, adapting this term that applies more intuitively to solutions to the atoms in crystalline solids. Neutron scattering and X-ray absorption fine structure (XAFS) measurements identified O-centered iqtps and their correlation with the superconductivity 30 y ago (17–25). We now present Cu K edge extended XAFS (EXAFS)

Significance

The Cu extended X-ray absorption fine structure of $YSr_2Cu_{2.75}Mo_{0.25}O_{7.54}$ (with superconducting critical temperature, T_c = 84 K) and $Sr_2CuO_{3.3}$ (T_c = 95 K) through their superconducting transitions demonstrates that the common factor in superconductivity in cuprates, including those prepared by high-pressure oxygenation, is an internal quantum tunneling polaron in its dynamical structure. In addition, $Sr_2CuO_{3.3}$ is the first material to show a concomitant transformation in this structure involving atom displacements >1 Å that would be expected to modify its Fermi surface, which would complicate the transition beyond a purely electronic one consisting of the pairing of electrons of opposite momentum across fixed electronic states.

Author contributions: S.D.C., T.H.G., and C.-Q.J. designed research; S.D.C., C.Q.-J., L.-P.C., A.G., M.K., G.B., W.-M.L., and J.M.J. performed research; L.-P.C., A.G., M.K., W.-M.L., E.G., M.L., O.M., and V.N. contributed new reagents/analytic tools; S.D.C., C.-Q.J., L.-P.C., A.G., M.K., G.B., and W.-M.L. analyzed data; and S.D.C., T.H.G., C.-Q.J., and E.G. wrote the paper.

Reviewers: A.B., Rome International Center for Materials Science Superstripes; J.M., Max Planck Institute for Solid State Research; and N.S., Sapienza University of Rome.

The authors declare no competing interest.

See online for related content such as Commentaries.

[1]To whom correspondence may be addressed. Email: st3v3n.c0nrads0n@icloud.com, geballe@stanford.edu, Jin@iphy.ac.cn, andrea.gauzzi@upmc.fr, or maarit.karppinen@aalto.fi.

This article contains supporting information online at https://www.pnas.org/lookup/suppl/doi:10.1073/pnas.2018336117/-/DCSupplemental.

First published December 14, 2020.

PHYSICS

results from "overdoped" $YSr_2Cu_{2.75}Mo_{0.25}O_{7.54}$ (YSCO-Mo) that is isostructural with $YBa_2Cu_3O_7$ (Fig. 1*A* and *SI Appendix*, Fig. S1), T_c = 84 K (26) and hole doping p (excess charge on the planar Cu2 site) = 0.3 to 0.5 (27) and $Sr_2CuO_{3.3}$ (SCO) that is structurally analogous to La_2CuO_4 (Fig. 1*B* and *SI Appendix*, Fig. S1), T_c = 95 K (28, 29), and p = 0.6, both synthesized via high-pressure oxygenation (HPO) (30, 31). In YSCO-Mo the Cu2-apical O (Oap) double-well potential is degenerate in the normal state but renormalizes below T_c with the energy difference between its two minima increasing with decreasing temperature by ∼6 meV. SCO is already unique among cuprates in not having intact CuO_2 planes (32, 33). Its Cu EXAFS demonstrate that it is unique among superconductors in that its Oap shift by >1 Å at its superconducting transition, challenging our conception of superconductivity as an electronic transition that is incompatible with structural transformations.

We have recently shown that HPO cuprates are described by their own phase diagram (34). The principal feature of the well-known one for non-HPO cuprates is the superconducting "dome"

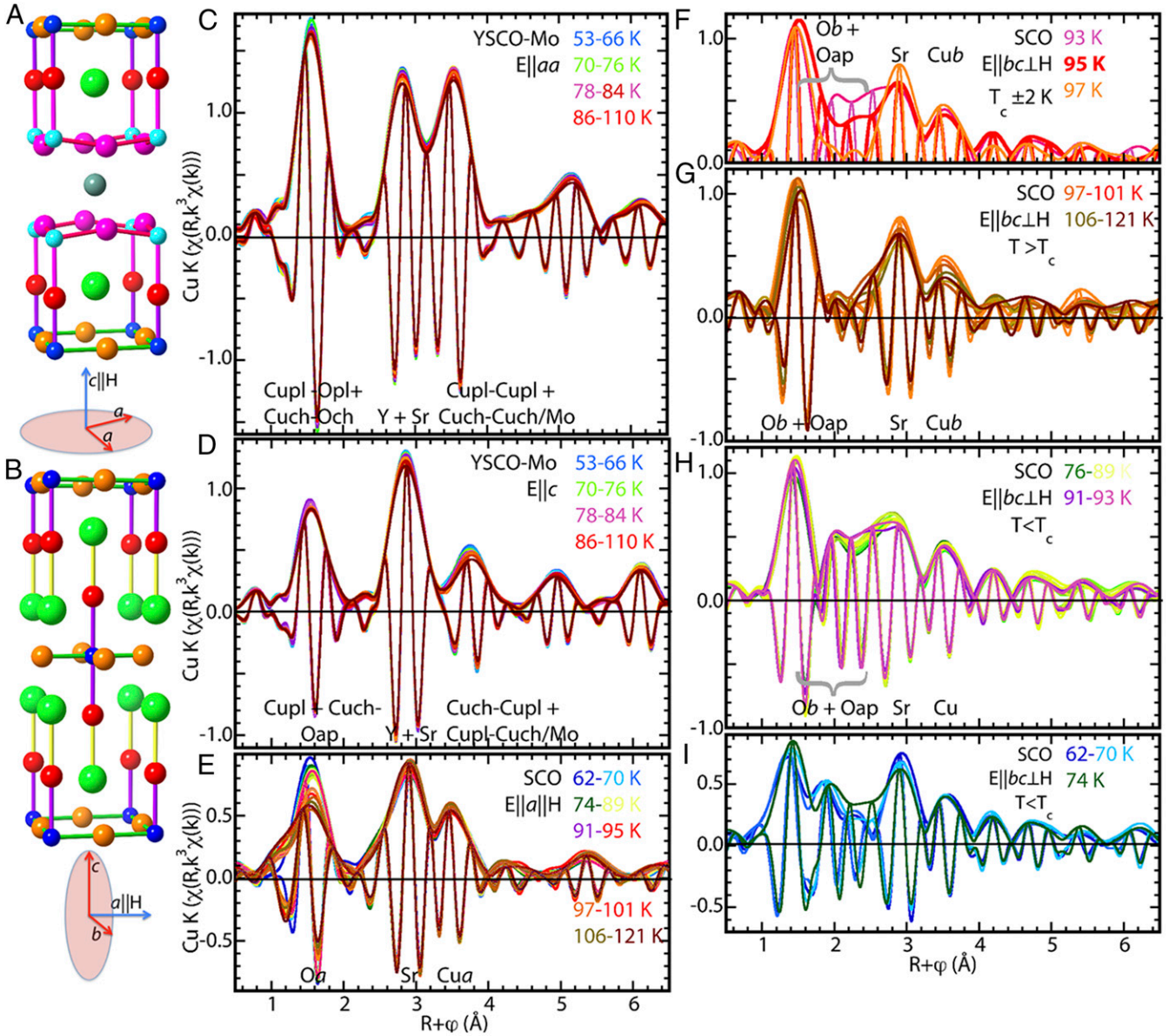

Fig. 1. Structures and modulus and real components of the Fourier transforms of the EXAFS spectra, χ(R), of YSCO-Mo and SCO across temperature ranges bracketing their superconducting transitions. (*A*) Structure representation of YSCO-Mo. The CuO_2 planes are turqoise (Cu2) and magenta (Opl), Cu-O chains are blue (Cu1) and gold (Och), Oap is red, and Sr is green. In the actual structure one-fourth of Cu1 are substituted by Mo. The orientation is shown underneath. (*B*) The same as *A* for SCO, except a significant number of Oap and half of the O sites in the *a* direction in the CuO_2 planes are vacant. The CuO_2 planes are blue (Cu) and gold (O). For the χ(R) spectra the blue traces denote the lowest temperatures, then green to yellow, purple, and red-orange to brown at the highest ones. (*C*) YSCO-Mo spectra for **E** of the X-ray probe beam in the *aa* plane, with the modulus peaks labeled with their principal sources. The first temperature above T_c is red. (*D*) YSCO-Mo spectra for **E**||*c*, with the Cu1- and Cu2-Oap contributions overlapping at R = 1.6 Å. The peaks at higher R are a combination of direct, two-leg path contributions from more distant neighbor atom shells and ordered multiple scattering paths. (*E*) SCO spectra for **E**||H used for the orientation that is assigned to the *a* direction of the orthorhombic O sublattice. T_c is red and double width. (*F–I*) SCO over the designated temperature ranges for **E**⊥H spectra that will be the contributions in the *bc* plane defined by the orthorhombic O sublattice. (*F*) The extent of the change in the spectra, and by inference in their originating structures, across the superconducting transition. The features appearing at R = 2 to 2.5 Å below T_c result from the ∼2 Å shift of the O depicted in Fig. 3 *B–D*. In *G* the first temperature above T_c is orange and double width.

that begins at p ~0.06, peaks at $p \sim 0.16$, and ends at $p \sim 0.27$. Subsequent augmentations with the microstrain in the planes (35) and hole density on the O atoms (36) explain some of the material specificity but do not modify this overall pattern. For HPO compounds the superconductivity may begin at $p < 0.06$ and continues to increase beyond $p = 0.27$ with possible flattening but no reduction in T_c. Although we have found that the excess O in YSCO-Mo is mostly taken up by domains enriched in octahedral Mo(VI) substituting in the Cu(1) chains, much of the extra charge resides in the CuO_2 planes (27) and some of the carriers constitute a normal Fermi liquid that coexists with the superconductivity (26). The inherent inhomogeneity (37) in YSCO-Mo and SCO was probed by EXAFS, which is arguably the most incisive experimental method for characterizing short-range order and is especially sensitive to its changes. Diffraction patterns originate in the long-range average structure of a material and provide precise information on the symmetry and symmetry-constrained locations of the atoms that dominate the Bragg peaks. In contrast, EXAFS—and pair distribution function (pdf) analysis—are sensitive to local order separate from the crystallographic symmetry. The element selectivity of EXAFS provides further advantages by separating the atom pairs comprising the distribution function. Especially important for this study, EXAFS measures the instantaneous structure factor, $S(Q, t = 0)$, that incorporates the dynamic structure components, $S(Q, E)$, observed with inelastic scattering. EXAFS therefore accesses time and energy scales corresponding to collective dynamical phenomena (25, 38, 39). Dynamical structures such as the iqtp are demonstrated when $S(Q, E/t = 0)$ gives locations for atoms that differ from those (19, 38) obtained from diffraction and elastic scattering measurements (20–22, 40). This complementarity was the basis for the original

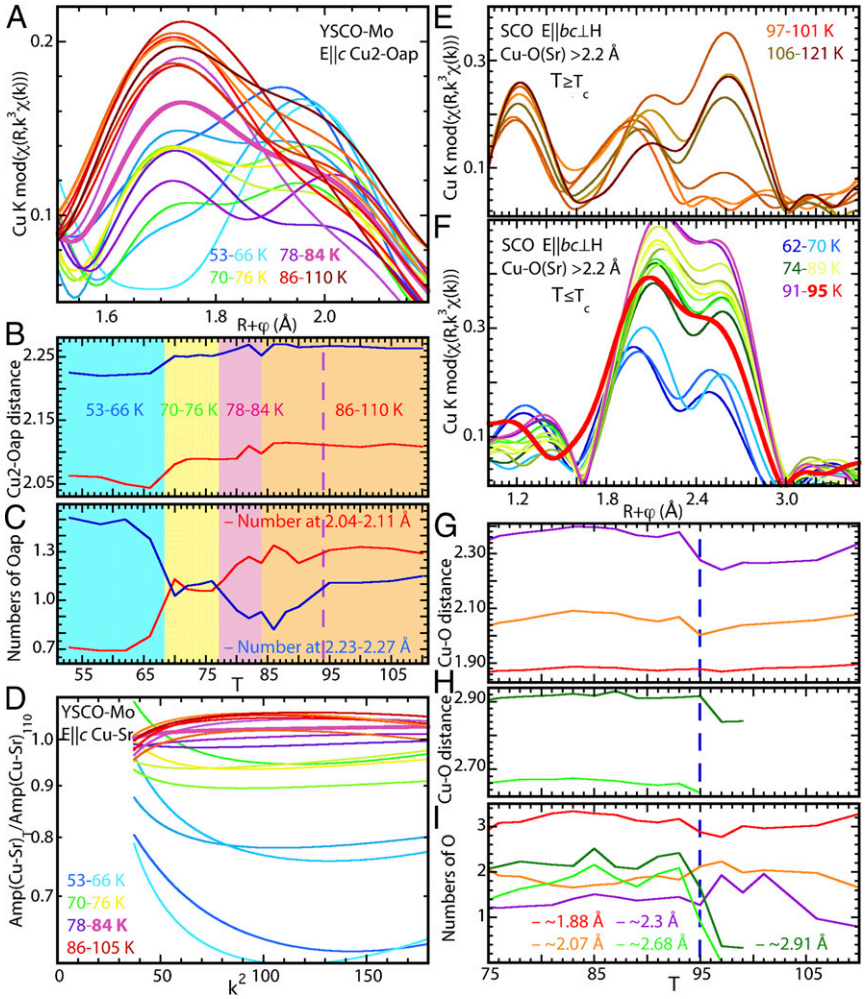

Fig. 2. Results characterizing the Cu2-Oap and Cu-Sr components of the dynamical structure of YSCO-Mo through its superconducting transition (*Left*) and the Cu-O *bc* oriented Cu-O pairs in SCO (*Right*). (*A*) Moduli of χ(R) of the isolated Cu2-Oap EXAFS spectra showing its two features at $R = 1.7$ and 1.95 Å. The color scheme is as in Fig. 1, with the $T_c \sim 84$ K curve in magenta plotted using a double-width line. (*B*) The two Cu2-Oap distances and (*C*) their corresponding numbers independently determined by curve fits of the EXAFS spectra (*SI Appendix*, Figs. S1–S40 and S71–S87). Discontinuous changes in these three values at the same temperatures divide the temperature range into the four regions, above T_c (orange), a fluctuation region (magenta) that begins at a somewhat higher temperature for the numbers (dashed line), below T_c (yellow), and farther below T_c (blue). The uncertainties for the three parameters can be taken as the SD from a line fit through the points in each region. (*D*) The anharmonicity of the Cu-Sr E||c pair, represented by the curvature of the logarithm of the ratio of the amplitude of the Cu-Sr wave at the designated temperatures divided by this amplitude at the maximum temperature of 110 K. (*E* and *F*) The corresponding χ(R) moduli of the isolated Cu-O waves for Cu-O > 2.1 Å, divided into above and below T_c because of the substantial change in the spectra and structure. The feature at $R = 2.6$ Å for T > 101 K is fit better by Sr than O, the one at $R = 2.5$ Å for T < 96 K is definitely O (*SI Appendix*, Fig. S87). (*G* and *H*) The Cu–O distances between 75 and 110 K with T_c indicated by the dashed blue line. (*I*) The numbers of O atoms at these distances, with the O at 2.68 and 2.91 Å appearing only below T_c because of the ~2-Å shift of the O as in Fig. 3 *B–D*.

identification of the Cu-Oap two-site distribution (41) and its assignment to the double-well potential of the iqtp (17, 19, 42).

Results

For YSCO-Mo one-fourth of the Cu1 atoms in the CuO_3 chain are replaced by Mo (26). The EXAFS of the sample of the $c||H||\mathbf{E}$ orientation of tetragonal YSCO-Mo is composed of the Cu1-Oap-Cu2 pairs and the *c*-axis projections of the Y/Sr pairs. The $(c||H)\perp(aa||\mathbf{E})$ sample contains the contributions of the CuO_2 planes–CuO_3 chains (34) and Y/Sr projections in the *aa* plane (Fig. 1*A* and *SI Appendix*, Fig. S1). Crystallographically tetragonal SCO (Fig. 1*B* and *SI Appendix*, Fig. S1) is unique in that its *a*-axis that contains half-filled -Cu-O- chains aligns with the field, its *b* axis in the *bc* plane perpendicular to the field contains intact -Cu-O- chains, and its Oap sites are only partly occupied (33). Its EXAFS corroborates that its Cu-Sr sublattice is locally tetragonal as found by diffraction.

The EXAFS spectra, $\chi(k)$, are presented as their Fourier transforms, $\chi(R)$, where the modulus peaks correspond to the contributions of the neighbor atom shells in an approximate representation of the partial pair distribution. This interpretation is modified by the phase shift that causes the locations of the modulus peaks to be below the actual distances and the finite data range that causes the peaks to be much wider than the actual resolving capability of the analysis. The overlap of the modulus peaks from adjacent neighbor shells therefore does not relate to the actual $\pi/2k_{max} = 0.11$ Å resolution in this analysis. Since the EXAFS signal includes both an amplitude and phase, the modulus represents only half of the information with the remainder contained in the real/imaginary component of $\chi(R)$. The $\mathbf{E}||aa$ (Fig. 1*C*) and $\mathbf{E}||c$ (Fig. 1*D*) spectra of YSCO-Mo are dominated by the contributions from the nearest-neighbor O, Sr, and Cu (34, 43–46). The increased thermal Debye–Waller factors at higher temperatures cause the small reductions in the amplitudes of the spectral features. Although the EXAFS spectra of SCO show the expected features from the nearest-neighbor O, Sr, and Cu, it differs from that of the La_2CuO_4 family (37, 47) since the spectra originate in the structures along the *a* axis and in the *bc* plane. In contrast to the expected behavior demonstrated by the YSCO-Mo spectra, the $\mathbf{E}||a$ spectra of SCO are complicated, showing a large reduction with increasing temperature for the Cu-O feature and an anomalous diminution of the Sr modulus amplitude with decreasing temperature (Fig. 1*E*).

The focus of this paper, however, is the behavior of the $\mathbf{E}||bc$ spectra of SCO in the region $R = 1.5$ to 2.8 Å that contains the contributions of Cu-O pairs at ∼2.2 to 3 Å. In contrast to the relatively subtle effects on the EXAFS resulting from the partial collapse of the iqtp double-well potential at T_c (20, 23, 42), these spectra have minimal amplitude in this region down to 97 K but at the onset of superconductivity at 95 K a complex pattern of large-amplitude features abruptly appears (Fig. 1*F*). This indicates the formation throughout the crystal of a structural moiety in the *bc* plane consisting of O ions displaced over long distances from their positions in the normal state into new ones in the superconducting state. That the crystal structure shows O atoms in symmetry-constrained positions that do not give these distances and no change in the structure across T_c (28, 29) indicates its dynamical origin. Smaller, continual changes divide the remaining spectra into temperature regions (Fig. 1 *G*, *J*, and *I*), demonstrating that the Cu environments undergo additional stepwise transformations.

Curve fitting (*SI Appendix*, Figs. S2–S70) confirms that the EXAFS gives the crystallographic positions for the cations and the YSCO-Mo plane and chain O atoms (33, 34). It also gives detailed depictions of the anomalous temperature dependence of Oap in YSCO-Mo and the entire O sublattice in SCO. The behavior of the Cu2-Oap in YSCO-Mo is visualized in the EXAFS of this pair isolated by subtracting the contributions of the other neighbors determined by the curve fits. The two-site distribution is evident in the two peaks in the residual $\chi(R)$ (Fig. 2*A*). The $R = 1.75$ Å peak increases continuously with increasing temperature, with a significant jump at T_c. The trend in position and amplitude of the $R = 1.95$ Å peak is more complicated, being relatively high at the lowest temperatures, then diminishing until near T_c it melds with the $R = 1.75$ Å one at a higher amplitude. This behavior reflects the sensitivity of $\chi(R)$ to the details of the two-site distribution, which are unraveled by the curve fits to reveal a consistent pattern. The two Cu–O distances and occupancies for the Cu2-Oap pair (Fig. 2 *B* and *C* and *SI Appendix*, Figs. S71–S86) divide into four regions: 1) the normal state for $T > 87$ K, 2) a fluctuation region from 77 to 85 K in the distances and 77 to 94 K in the numbers of the two O, 3) a first superconducting region from 68 to 77 K, and 4) a second superconducting region for $T < 68$ K. Although the distances and numbers are all obtained independently, the stepwise shifts in distances and numbers occur at the same temperatures, delineating the boundaries of temperature regions where the two-site distribution and its double-well potential change.

Another quantity showing coupling to the superconductivity is the anharmonicity of the *c*-oriented Cu2-Sr pair. This is evaluated from the EXAFS from the logarithm of the amplitude divided by the amplitude of the selected baseline spectrum vs. k^2 (Fig. 2*D*). Since the Cu-Sr sublattice is conserved the linear part of this function is the difference in the Gaussian Debye–Waller factor and the curvature and deviation of the intercept from zero reflects the change in the anharmonic component of the pair distribution (48). The conservation of the Cu-Sr distribution in the normal state is demonstrated by these ratios being essentially horizontal lines with extrapolated intercepts of 1 from 85 to 110 K. At T_c these ratios begin to decrease continuously, at a faster rate and with greater curvature as the temperature becomes lower. This pattern implies that the polarizability of the Sr scales with the superfluid density.

The most remarkable component in the structure of SCO is the entity that forms in the *bc* plane at T_c to give the spectral features at $R = 1.8$ to 2.6 Å in the superconducting phase. Curve fits confirm the absence of significant numbers of O neighbors beyond 2.4 Å in the normal state. Subtracting the contributions of the two O neighbors with Cu–O distances <2 Å and the Sr and Cu visualizes the relevant portion of the spectrum (49) (Fig. 2 *E* and *F*). The radical change in the full spectrum from 93 to 97 K is the result of a reduction in the amplitude of the feature at $R = 2.0$ Å to half its size at T_c and a complete loss of the feature around $R = 2.6$ Å in the normal phase (Fig. 2 *E* and *F*). The shifts of the lower feature and the recovery of the higher one beginning at 106 K is complicated and may result from the displacement of an Sr atom rather than the resumption of the 93 K structure (*SI Appendix*, Fig. S88). Below T_c the overall shape is retained, albeit with shifts in the positions of the peaks, and the amplitude that is at a maximum just below T_c diminishes, with a large reduction between 74 and 70 K (Fig. 2*F*). The spectrum in this region is fit by an O neighbor around 2.3 Å and larger, approximately equivalent numbers of O neighbors with Cu–O distances of 2.6 Å and 2.9 Å in the *bc* plane (Fig. 2*G*, *H*, and *I* and *SI Appendix*, Figs. S56–S70). These two neighbors are not present in the normal phase (Fig. 2*I*) and must result from a large displacement of an O atom from one position in the lattice to another. The other changes occurring at the transition are the substantial reduction in the amplitude of the O at 2.3 Å along with the 0.13 Å expansion of its Cu–O distance and a 0.06 Å expansion of the Cu–O at 2.05 Å.

Discussion

Descriptions of the structural transformations in YSCO-Mo and SCO consistent with these results begin with the previously described environments of the relevant O atoms (33, 34) (Fig. 3).

The two-site apical O distribution in YSCO-Mo is simple (Fig. 3*A*), here showing the positions synchronized along the chain. SCO is much more complex. Interpreting the high degree of disorder and the large change at T_c as a random distribution of the apical and chain vacancies, there are three types of Cu, all with two *b* chain but distinguished by having zero, one, or two *a* chain O neighbors. The square planar geometry of Cu(II) dictates that the $2a+2b$ conformation would have its Oap either vacant or with one or two Oap at >2.1 Å and the $0a+2b$ conformation two Cu-Oap distances at <2 Å. The $1a+2b$ Cu with its long or short Cu-Oap and distorted environment would then be the Cu(III) required for charge balance. This combination of occupied and vacant Oap sites explains the EXAFS spectra of the normal phase, with the low Cu-Oap amplitude caused by the range of Cu-Oap distances (Fig. 3*B*). At T_c an Oap adjacent to an Oap-vacancy shifts ∼2 Å in the *b* direction to form a Cu_2O_2 unit with an asymmetric bridge that gives the Cu–O distances of 2.6 and 2.9 Å (Fig. 3 *C* and *D*). The other O of the Cu_2O_2 shifts along *c* away from this Oap, buckling the original -Cu-O-Cu- chain. This O would also move away from the Cu with the shorter, 2.6 Å Cu–O distance, splitting the original distance into two distances at 1.85 and 2.05 Å. The expansion of the 2.05 Å Cu–O distances at T_c would therefore be a response to the formation of these asymmetrically bridged Cu_2O_2 units. The expansion of the 2.3 Å distance assigned to a long Cu-Oap (Fig. 3*G*) would result from the modified charge distribution and the increased homogeneity of the Cu sites, whereby ones with and without Oap become more uniform. The 1.9-Å Cu–O distances are unaffected because they are not involved in this transformation.

Analogous to $YBa_2Cu_3O_7$, the Cu2-Oap two-site distribution in YSCO-Mo is assigned to the iqtp of the dynamical structure. This is corroborated by the single site distribution found for Cu1-Oap that shows that the correlated motion of the Cu2-Oap pair differs from the Cu1-Oap pair. Assignment of the asymmetrically bridged Cu_2O_2 unit in superconducting SCO to an iqtp is supported by the difference with the crystallographic structure determined by neutrons (28, 29) that also show no change across T_c. The dynamical component of the iqtp would be the oscillation of the O atoms between their two equivalent positions across the Cu_2O_2 midpoint.

Iqtps coupled to the superconductivity are the first significant finding of this paper. Recent reports by the authors have shown that the common attribute in cuprate superconductivity is not the superconducting "dome" of the phase diagram(34) or CuO_2 planes (33) or the prolate geometry of the Cu in these planes (50). A remaining factor is the dynamical structure of specific Cu-O pairs, the iqtps. The identification of iqtps as a ubiquitous factor in exotic superconductivity follows from their identification by EXAFS measurements in all classes of cuprates, $La_{2-x}Ba/Sr_xCuO_{4+\delta}$ (42, 47, 51–53), $YBa_2Cu_3O_7$ (20, 46), Bi- and Tl-based layered cuprates (23, 24, 54, 55), and even related Bi- and Fe-based compounds (56–58). The basis for this superiority of EXAFS for revealing iqtps is unclear—perhaps it is simply easier than neutron pdf measurements—but it is empirically incontrovertible. YSCO-Mo and SCO therefore exemplify the prevalence of the iqtp even under constraint. The Cu1-Oap iqtp in $YBa_2Cu_3O_7$ wholly switches to Cu2-Oap when obstructed by the 25% Cu1-Mo substitution of YSCO-Mo, and in disordered SCO the host Cu_2O_2 unit forms at T_c by an ∼2-Å lateral displacement of an Oap.

EXAFS has previously identified iqtps in both the Oap and the CuO_2 planes (52, 53, 55). Their appearance concomitant with the (PG) at T* is explained as the initial freezing out of polarons that in underdoped cuprates self-assemble into the PG and other aggregates (25, 59). Their response to the reduction of T_c by compositional changes that repress both polarons and superconductivity implicate them in the pairing-condensation process (42). The iqtps have the following additional properties that are independent of their location as Oap or in the planes, their host compound, and the Cu–Oap distance. Namely, 1) with the exception of SCO, the separation of the two Cu–O distances is 0.14 to 0.18 Å, 2) the double-well potential collapses at T_c but is subsequently restored as the temperature is further lowered, 3) the change in energy calculated from their tunneling frequencies or relative occupancies is 5 to 15 meV (25), 4) and at optimum doping they constitute 60 to 100% of the sites in the crystal. These common characteristics imply that the iqtp is largely a property of the O and the Zhang–Rice singlet state that occurs on Oap despite the $3d_z2$ level's being lower in energy than the $3d_x2_{-y}2$. However, the relationship of the iqtp to the superfluid quasiparticles is unclear insofar as, pending more complete data, the forms and populations of the double-well potentials do not appear to track the phase diagram with the exception of the softening at T_c.

The second remarkable result is the ∼2-Å displacement in the dynamic structure of Oap coincident with the superconducting transition. Changes in the structure across T_c in response to charge screening by the superfluid are only a few parts per thousand in the lattice constants of conventional BCS-type superconductors. Percent shifts occur in the Cu2-Oap distributions in cuprates. The O displacement in SCO would be the first observation of a rearrangement of the atoms sufficiently large to effect a change in the Fermi surface at the transition. This is a substantial departure from the standard depiction of BCS as a pairing of electrons of opposite momentum across a conserved Fermi surface in which the mediation of this pairing by a soft lattice mode prevents that mode from providing a path for a structural transformation. The caveat in this result is that this transformation occurs in the dynamic and not the static structure. Recent inelastic neutron scattering results in other systems have confirmed that such structural features demonstrate dynamic pair correlations not present in the static structures that originate in processes such as tunneling (39). An outstanding question is the effects of the HPO synthesis that results in compounds displaying a very much different superconducting region in their phase diagram than the "dome" of conventional cuprates prepared with O_2 (34, 60). The 84 K T_c of YSCO-Mo, which EXAFS shows conforms very closely to the typical structure of cuprates without substantial disorder, is one-third higher than that of its parent $YSr_2Cu_3O_{7+\delta}$ despite a measured *p* of 0.5 (27). It nevertheless possesses the same two-site Cu-Oap distribution found in other cuprates, differing in that the relative occupancies change instead of converging at T_c. The 95 K T_c of this phase of $Sr_2CuO_{3.3}$ is over 2.5 times higher than its $La_{1.85}Sr_{0.15}CuO_4$ structural analog (32). Its unique Cu charge, structure, magnetism, and very high degree of disorder in its O sublattice (33) could be expected to convey additional unique behaviors, for example the structural transformation we have identified and described here.

These results provide evidence for a direct role in cuprates for nonadiabatic lattice dynamics that manifests itself as anharmonic oscillations of the atoms and charges (61) coupled to the superconductivity. Analogous to, for example, monolayer FeSe on $SrTiO_3$ (62) and Li_2CuO_2 (63), our analysis demonstrates that collective behaviors of iqtps most likely have an equally significant role in pairing and condensation. For the iqtp, this collective action is easily assigned to the dynamic synchronization of the O oscillations over distances of the order of the superconducting coherence length. The interaction of the oscillators occurs not only through their dipoles but also directly through their neighbors, for example the Sr that bridges the Oap atoms in YSCO-Mo. Oscillating charge and a significant role for the inert cations have not been previously reported or proposed. In addition, the dynamical structure we report here is of substantial interest as a mechanism for the collective integration of lattice dynamics and charge that derives from a charge-coupled structural instability

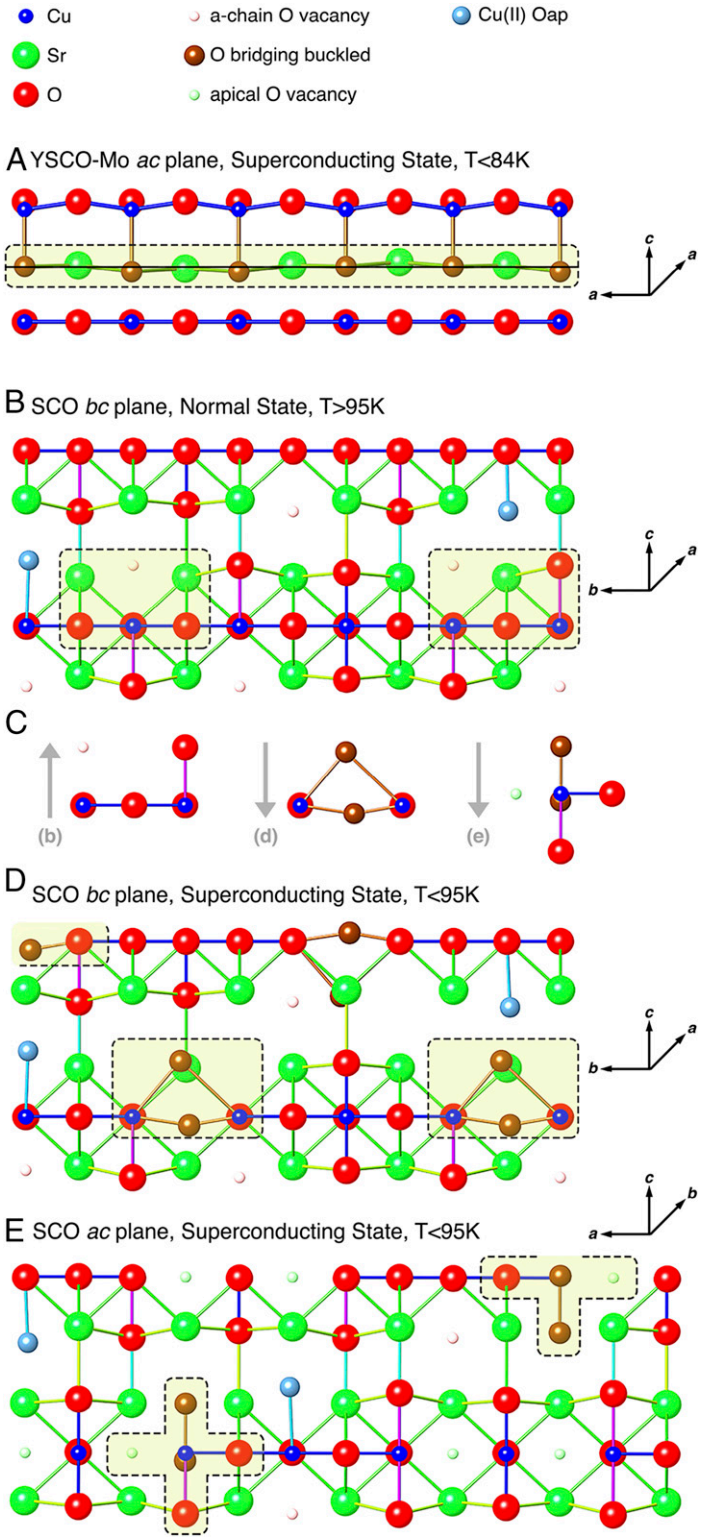

Fig. 3. Conceptual structures of the dynamical structure transformations. The results from SCO are derived from the EXAFS results. The shaded areas highlight the atoms of the iqtps whose structure will change across T_c. (*A*) Cu2-Oap two-site distribution in YSCO-Mo, organized in pairs with corresponding displacements of the Sr. (*B*) The *bc* plane in the normal state of SCO. There are some Oap vacancies, and the *b*-oriented Cu-O chains are fully occupied. As described in the text the half-vacant O sites in the *a*-oriented Cu-O chains give three types of Cu: 1) zero O along *a*, two O along *b*, two Oap with Cu-Oap ~1.9 Å; 2) two O along *a*, two O along *b*, 0 to 2 Oap with Cu-Oap > 2.1 Å; and 3) Cu(III) with one O along *a*, two O along *b*, and variable Oap. (*C*) The Cu_2O_2 unit in SCO whose structure changes across T_c. (*Left*) In the *bc* plane in the normal state (*B*) showing the two Cu sites, one of which has an O vacancy in the *a* direction, and one with an Oap vacancy. In the superconducting state (*Center, D*) the Oap has shifted toward the Oap vacancy to give the 2.7- and 2.9-Å Cu–O distances and the O in the Cu has moved slightly downward. (*Right*) The same set of atoms viewed in the *ac* plane as in *E*. (*D*) The *bc* plane in the superconducting state of SCO, showing the doubly bridged Cu_2O_2 units. (*E*) The *ac* plane in the superconducting state of SCO, showing the three types of Cu.

that does not culminate in static transformation. It is thereby consistent with the original rationale for superconductivity in cuprates, stabilizing the Cooper pairs by increasing the electron–lattice coupling beyond the adiabatic approximation while simultaneously frustrating incipient structural phase transitions (1, 5), but also constitutes a significant extension to high temperature superconductivity.

Materials and Methods

The samples, data acquisition, and analysis are the same as in our recent reports (33, 34) with the addition of having been measured at multiple temperatures and are detailed in *SI Appendix*. The two compounds were synthesized and samples prepared by magnetic orientation and characterized by standard methods as described in those reports and others that they cite. XAFS measurements were performed at the Stanford Synchrotron Light Source in the continuous scanning transmission mode on end station 2-2. χ(k) spectra were obtained after the standard energy calibration, conversion to absorbance, normalization, and approximation of the smooth atomic background with a sum of a fraction of the absorption peak at the edge plus a spline polynomial with a sufficiently low number of knots and polynomial orders to avoid fitting EXAFS oscillations and that minimized frequencies lower than those of the structural features. The spline parameters were also held to narrow ranges within each of the four sets of spectra to ensure the absence of any artifacts from this procedure. Metrical parameters were obtained by curve fitting of the χ(k) data using amplitudes and phases calculated with the feff9 code (64). Debye–Waller factors and E_0 values were constrained to narrow ranges determined by inspection of the results from unconstrained fits on the spectra from all temperatures. Debye–Waller factors for the separable Cu-neighbors pairs were also evaluated by the logarithm-amplitude ratio method as in Fig. 2*D*, often showing analogous correlations with the superconducting transition. These will be reported later.

Data Availability. In the absence of an appropriate institutional open access data repository, the original data can be obtained by contacting the first author at st3v3n.c0nrads0n@icloud.com.

ACKNOWLEDGMENTS. We acknowledge the financial support from the Slovenian Research Agency (research core funding no. P1-0040). Work at Washington State University is partially supported by the US National Science Foundation Division of Materials Research Early Concept Grants for Exploratory Research Grant 1928874. Work at Institute of Physics, Chinese Academy of Sciences was supported by the Ministry of Science and Technology and National Natural Science Foundation of China. Use of the Stanford Synchrotron Radiation Lightsource, SLAC National Accelerator Laboratory, is supported by the US Department of Energy, Office of Science, Office of Basic Energy Sciences under Contract DE-AC02-76SF00515. Work at Stanford and SLAC is supported by the Stanford Institute for Materials and Energy Sciences, SLAC National Accelerator Laboratory, under Department of Energy, Office of Basic Energy Sciences Contract DEAC02-76SF00515. We thank A. R. Bishop, I. Bozovic, A. Bussmann-Holder, S. A. Kivelson, D. Mihailovic, and C. Varma for helpful discussions and presubmssion reviews of this manuscript.

1. J. G. Bednorz, K. A. Muller, Possible high T_c superconductivity in the Ba-La-Cu-O system. *Z. Phys. B Condens. Matter* **64**, 189–193 (1986).
2. B. Keimer, S. A. Kivelson, M. R. Norman, S. Uchida, J. Zaanen, From quantum matter to high-temperature superconductivity in copper oxides. *Nature* **518**, 179–186 (2015).
3. A. Bussmann-Holder *et al*., The road map toward room-temperature superconductivity: Manipulating different pairing channels in systems composed of multiple electronic components. *Condens. Matter* **2**, 24 (2017).
4. I. Bozovic, X. He, J. Wu, A. T. Bollinger, The vanishing superfluid density in cuprates-and why it matters. *J. Supercond. Nov. Magn.* **31**, 2683–2690 (2018).
5. A. Bussmann-Holder, H. Keller, Isotope and multiband effects in layered superconductors. *J. Phys. Condens. Mat.* **24**, 233201 (2012).
6. A. Shekhter *et al*., Bounding the pseudogap with a line of phase transitions in $YBa_2Cu_3O_{6+\delta}$. *Nature* **498**, 75–77 (2013).
7. A. Lanzara *et al*., Evidence for ubiquitous strong electron-phonon coupling in high-temperature superconductors. *Nature* **412**, 510–514 (2001).
8. S. Johnston *et al*., Systematic study of electron-phonon coupling to oxygen modes across the cuprates. *Phys. Rev. B Condens. Matter Mater. Phys.* **82**, 064513 (2010).
9. Y. He *et al*., Rapid change of superconductivity and electron-phonon coupling through critical doping in Bi-2212. *Science* **362**, 62–65 (2018).
10. A. Pashkin *et al*., Femtosecond response of quasiparticles and phonons in superconducting YBa_2 Cu_3 $O_{7-\delta}$ studied by wideband terahertz spectroscopy. *Phys. Rev. Lett.* **105**, 067001 (2010).
11. T. Konstantinova *et al*., Nonequilibrium electron and lattice dynamics of strongly correlated $Bi_2Sr_2CaCu_2O_{8+\delta}$ single crystals. *Sci. Adv.* **4**, p7427 (2018).
12. A. Cavalleri, Photo-induced superconductivity. *Contemp. Phys.* **59**, 31–46 (2018).
13. A. Bianconi, M. Filippi, "Feshbach shape resonances in multiband high T_c superconductors" in *Symmetry and Heterogeneity in High Temperature Superconductors*, A. Bianconi, Ed. (Springer, 2006), 214, pp. 21–53.
14. J. Chang *et al*., Direct observation of competition between superconductivity and charge density wave order in $YBa_2Cu_3O_{6.67}$. *Nat. Phys.* **8**, 871–876 (2012).
15. Y. He *et al*., Persistent low-energy phonon broadening near the charge-order q vector in the bilayer cuprate $Bi_2Sr_2CaCu_2O_{8+\delta}$. *Phys. Rev. B* **98**, 035102 (2018).
16. M. Hashimoto *et al*., Direct spectroscopic evidence for phase competition between the pseudogap and superconductivity in $Bi_2Sr_2CaCu_2O_{(8+\delta)}$. *Nat. Mater.* **14**, 37–42 (2015).
17. M. de Leon J, I. Batistic, A. R. Bishop, S. D. Conradson, S. A. Trugman, Polaron origin for anharmonicity of the axial oxygen in $YBa_2Cu_3O_7$. *Phys. Rev. Lett.* **68**, 3236–3239 (1992).
18. M. de Leon J, M. I. Salkola, A. R. Bishop, S. A. Trugman, Dynamic polaron tunneling in $YBa_2Cu_3O_7$: Optical response and inelastic neutron scattering. *Phys. Rev. B Condens. Matter* **49**, 3671–3674 (1994).
19. J. M. DeLeon *et al*., "X-ray absorption fine structure applied to the study of systems with lattice instabilities" in *Applications of Synchrotron Radiation Techniques to Materials Science III*, L. J. Terminello, S. M. Mini, H. Ade, D. L. Perry, Eds. (Cambridge University Press, 1996), vol. 437, pp. 189–199.
20. S. D. Conradson, I. D. Raistrick, A. R. Bishop, Axial oxygen-centered lattice instabilities and high-temperature superconductivity. *Science* **248**, 1394–1398 (1990).
21. T. Egami *et al*., Local structural anomaly near T_c observed by pulsed neutron-scattering. *Physica C* **185**, 867–868 (1991).
22. M. Arai *et al*., Local structural instability of high-T_c oxide superconductors studied by inelastic neutron-scattering. *J. Supercond.* **7**, 415–418 (1994).
23. P. G. Allen, S. D. Conradson, A. R. Bishop, M. de Leon J, Characterization of a split axial-oxygen site in $TlBa_2Ca_3Cu_4O_{11}$ by extended x-ray-absorption fine-structure spectroscopy. *Phys. Rev. B Condens. Matter* **44**, 9480–9485 (1991).
24. J. M. Deleon *et al*., Planar oxygen-centered lattice instabilities in Tl-based high-temperature superconductors. *Physica C* **220**, 377–382 (1994).
25. A. R. Bishop, D. Mihailovic, J. M. de Leon, Signatures of mesoscopic Jahn-Teller polaron inhomogeneities in high-temperature superconductors. *J. Phys. Condens. Matter* **15**, L169–L175 (2003).
26. A. Gauzzi *et al*., Bulk superconductivity at 84 K in the strongly overdoped regime of cuprates. *Phys. Rev. B* **94**, 180509 (2016).
27. I. Grigoraviciute *et al*., Electronic structures, hole-doping, and superconductivity of the s = 1, 2, 3, and 4 members of the (Cu,Mo)-12*s*2 homologous series of superconductive copper oxides. *J. Am. Chem. Soc.* **132**, 838–841 (2010).
28. Q. Q. Liu *et al*., Enhancement of the superconducting critical temperature of $Sr_2CuO_{3+\delta}$ up to 95 K by ordering dopant atoms. *Phys. Rev. B* **74**, 100506(R) (2006).
29. Y. Liu *et al*., A new modulated structure in $Sr_2CuO_{3+delta}$ superconductor synthesized under high pressure. *Physica C* **497**, 34–37 (2014).
30. A. Ono, Oxygenation and critical-temperature optimization in M-1212 cuprates (*Sr*, *Ba*)$_2YCu_{2.8}M_{0.2}O_z$ (M = Ti, Ga, Ge, Al). *Jpn. J. Appl. Phys., Part 2* **35**, L201–L204 (1996).
31. J. M. S. Skakle, Crystal chemical substitutions and doping of $YBa_2Cu_3O_x$ and related superconductors. *Mater. Sci. Eng. Rep.* **23**, 1–40 (1998).
32. T. H. Geballe, M. Marezio, Enhanced superconductivity in Sr_2CuO_{4-v}. *Physica C* **469**, 680–684 (2009).
33. S. D. Conradson *et al*., Local structure of $Sr_2CuO_{3.3}$, a 95 K cuprate superconductor without CuO_2 planes. *Proc. Natl. Acad. Sci. U.S.A.* **117**, 4565–4570 (2020).
34. S. D. Conradson *et al*., Local lattice distortions and dynamics in extremely overdoped superconducting $YSr_2Cu_{2.75}Mo_{0.25}O_{7.54}$. *Proc. Natl. Acad. Sci. U.S.A.* **117**, 4559–4564 (2020).
35. S. Agrestini, N. L. Saini, G. Bianconi, A. Bianconi, The strain of CuO2 lattice: The second variable for the phase diagram of cuprate perovskites. *J. Phys. Math. Gen.* **36**, 9133–9142 (2003).
36. D. Rybicki, M. Jurkutat, S. Reichardt, C. Kapusta, J. Haase, Perspective on the phase diagram of cuprate high-temperature superconductors. *Nat. Commun.* **7**, 11413 (2016).
37. G. Fabbris, M. Hucker, G. D. Gu, J. M. Tranquada, D. Haskel, Combined single crystal polarized XAFS and XRD at high pressure: Probing the interplay between lattice distortions and electronic order at multiple length scales in high T_c cuprates. *High Press. Res.* **36**, 348–359 (2016).
38. M. I. Salkola, A. R. Bishop, S. A. Trugman, J. M. Deleon, M. de Leon J, Correlation-function analysis of nonlinear and nonadiabatic systems: Polaron tunneling. *Phys. Rev. B Condens. Matter* **51**, 8878–8891 (1995).
39. W. Dmowski *et al*., Observation of dynamic atom-atom correlation in liquid helium in real space. *Nat. Commun.* **8**, 15294 (2017).
40. C. A. Young *et al*., Reverse Monte Carlo study of apical Cu-O bond distortions in $YBa_2Cu_3O_{6.93}$. *Z. Kristallogr. Cryst. Mater.* **227**, 280–287 (2012).
41. S. D. Conradson, I. Batistic, A. R. Bishop, M. de Leon J, Evidence for an axial oxygen-centered lattice fluctuation associated with the superconducting transition in $YBa_2Cu_3O_7$. *Phys. Rev. Lett.* **65**, 1675–1678 (1990).
42. H. Oyanagi, C. Zhang, A. Tsukada, M. Naito, Lattice instability in high-temperature superconducting cuprates: Polarons probed by EXAFS. *J. Supercond. Nov. Magn.* **22**, 165–168 (2009).
43. K. Zhang *et al*., Extended x-ray-absorption fine-structure experiment on the high-*Tc* superconductor $YBa_2Cu_3O_{7-\delta}$. *Phys. Rev. B Condens. Matter* **37**, 3375–3380 (1988).

44. J. Whitmore *et al*., XAFS of oriented single-crystal of $YBa_2Cu_3O_{7-x}$. *Physica B* **158**, 440–442 (1989).
45. J. B. Boyce, F. Bridges, T. Claeson, Local-structure of high-temperature superconductors from x-ray absorption studies. *Phys. Scr. T* **42**, 71–75 (1992).
46. C. H. Booth *et al*., Comparison of local structure measurements from c-axis polarized XAFS between a film and a single crystal of $YBa_2Cu_3O_{7-\delta}$ as a function of temperature. *Phys. Rev. B Condens. Matter* **54**, 9542–9554 (1996).
47. M. Acosta-Alejandro, J. M. de Leon, S. D. Conradson, A. R. Bishop, Evidence for a local structural change in $La_2CuO_{4.1}$ across the superconducting transition. *J. Supercond.* **15**, 355–360 (2002).
48. G. Bunker, Application of the ratio method of EXAFS analysis to disordered systems. *Nucl. Instrum. Methods Phys. Res.* **207**, 437–444 (1983).
49. S. D. Conradson *et al*., Nanoscale heterogeneity, premartensitic nucleation, and a new plutonium structure in metastable delta fcc Pu-Ga alloys. *Phys. Rev. B Condens. Matter Mater. Phys.* **89**, 224102 (2014).
50. W. M. Li *et al*., Superconductivity in a unique type of copper oxide. *Proc. Natl. Acad. Sci. U.S.A.* **116**, 12156–12160 (2019).
51. A. Bianconi *et al*., Determination of the local lattice distortions in the CuO_2 plane of $La_{1.85}Sr_{0.15}CuO_4$. *Phys. Rev. Lett.* **76**, 3412–3415 (1996).
52. J. M. de Leon, M. Acosta-Alejandro, S. D. Conradson, A. R. Bishop, Change of the in-plane Cu–O bond distribution in $La_2CuO_{4.1}$ across T_c. *J. Phys. Chem. Solids* **69**, 2288–2291 (2008).
53. C. J. Zhang, H. Oyanagi, Local lattice instability and superconductivity in $La_{1.85}Sr_{0.15}Cu_{1-x}M_xO_4$ (M = Mn, Ni, and Co). *Phys. Rev. B Condens. Matter Mater. Phys.* **79**, 064521 (2009).
54. A. Bianconi *et al*., Stripe structure in the CuO2 plane of perovskite superconductors. *Phys. Rev. B Condens. Matter* **54**, 12018–12021 (1996).
55. S. D. Conradson, J. M. DeLeon, A. R. Bishop, Local phase separation in Tl-based oxide superconductors. *J. Supercond.* **10**, 329–332 (1997).
56. A. P. Menushenkov, K. V. Klementev, Extended x-ray absorption fine-structure indication of a double-well potential for oxygen vibration in $Ba_{1-x}K_xBiO_3$. *J. Phys. Condens. Matter* **12**, 3767–3786 (2000).
57. S. D. Conradson *et al*., Possible Bose-condensate behavior in a quantum phase originating in a collective excitation in the chemically and optically doped Mott-Hubbard system UO_{2+x}. *Phys. Rev. B Condens. Matter Mater. Phys.* **88**, 115135 (2013).
58. V. G. Ivanov, A. A. Ivanov, A. P. Menushenkov, B. Joseph, A. Bianconi, Fe-As bond fluctuations in a double-well potential in LaFeAsO. *J. Supercond. Nov. Magn.* **29**, 3035–3039 (2016).
59. T. Mertelj, V. V. Kabanov, D. Mihailovic, Charged particles on a two-dimensional lattice subject to anisotropic Jahn-Teller interactions. *Phys. Rev. Lett.* **94**, 147003 (2005).
60. M. Marezio *et al*., Overdoped cuprates with high-temperature superconducting transitions. *APL Mater.* **1**, 021103 (2013).
61. X. Chen, J. Dong, X. Li, A picture of pseudogap phase related to charge fluxes. *Npj Comput. Mater.* **6**, 103 (2020).
62. S. Y. Zhang *et al*., Enhanced superconducting state in $FeSe/SrTiO_3$ by a dynamic interfacial polaron mechanism. *Phys. Rev. Lett.* **122**, 066802 (2019).
63. S. Johnston *et al*., Electron-lattice interactions strongly renormalize the charge-transfer energy in the spin-chain cuprate Li_2CuO_2. *Nat. Commun.* **7**, 10563 (2016).
64. J. J. Rehr, J. J. Kas, F. D. Vila, M. P. Prange, K. Jorissen, Parameter-free calculations of X-ray spectra with FEFF9. *Phys. Chem. Chem. Phys.* **12**, 5503–5513 (2010).